



Lift Enhancement of High Angle of Attack Airfoils Using Periodic Pitching

Scott T. M. Dawson*, Daniel C. Floryan[†] and Clarence W. Rowley[‡]

Princeton University, Princeton, NJ 08544

Maziar S. Hemati[§]

University of Minnesota, Minneapolis, MN 55455

In this work, we study a sinusoidally pitching, two-dimensional flat plate airfoil at a Reynolds number of 100, across a range of pitching amplitudes, frequencies, mean angles of attack, and pitch axis locations. We report on the lift, drag, and wake structures present in different regions of parameter space. We examine the average and spectral properties of the forces on the airfoil, and use dynamic mode decomposition to examine the structures and frequency content of the wake. We give focus to a number of regions in parameter space where interesting behavior is observed. In particular, we find that in the regime where the flow on the upper surface of the airfoil is separated, but the steady wake is stable, pitching at a specific frequency excites a vortex shedding mode in the wake, leading to substantial increase in the lift and drag forces. This phenomena is insensitive to pitch-axis location and amplitude. At higher angles of attack where the wake for a steady airfoil exhibits periodic vortex shedding, we find that, in addition to this mean lift maxima, the interaction between the natural and forced modes gives rise to more complex behavior.

I. Introduction

The unsteady motion of airfoils at low Reynolds number and high angle of attack leads to a range of phenomena that cannot adequately be explained by classical aerodynamic theories. It is precisely these conditions that are encountered by small fliers, ranging from biological examples such as birds,¹ insects,^{2,3,4} and bats, or manmade UAVs and MAVs. The vortex dynamics excited by airfoil motion, actuation, or indeed present in the natural flow at sufficiently high angles of attack, can significantly affect aerodynamic performance.⁵ This motivates work that seeks to understand and control such phenomena, and indeed modeling the dynamics of pitching and plunging airfoils has attracted significant recent attention.^{6,7,8,9,10,11,12}

This work will investigate the interaction between periodic vortex shedding that can occur for bluff bodies (or airfoils at sufficiently large angle of attack), and imposed sinusoidal pitching motion. In the case of plunging motion, it has been observed that lock on¹³ can occur between plunging frequency and natural vortex shedding,^{14,15,16} while similar phenomena have been found for surging oscillations over a wide range of Reynolds number.¹⁷ We will show that similar phenomena are observed in the case of pitching motion. In experimental conditions, plunging oscillations may also lead to a bifurcation of the wake direction.¹⁸

It has been observed that optimal pitching trajectories maximize the circulation that is entrained in leading edge vortices,¹⁹ linking the concepts explored here to the general notion of a formation number that can be used to explain characteristic sizes and frequencies associated with vortex phenomena.²⁰

While this work will only consider two-dimensional airfoils, we note that three dimensional phenomena can give rise to additional complexity. For example, aspect ratio effects being significant on lift enhancement due to periodic forcing,²¹ and in the case of three dimensional airfoils that are free to exhibit rolling motion, forced pitching can lead to self-excited roll oscillations.²²

*Graduate Student, Department of Mechanical and Aerospace Engineering; AIAA Student Member.

[†]Graduate Student, Department of Mechanical and Aerospace Engineering.

[‡]Professor, Department of Mechanical and Aerospace Engineering; AIAA Associate Fellow.

[§]Assistant Professor, Aerospace Engineering and Mechanics; AIAA Member.

There are strong parallels between studying the effect on lift and drag in the context of lifting airfoils, and in the investigation of thrust-generating airfoils,²³ where it is found that propulsive efficiency is maximized when flapping produces a reverse von-Kàrmàn wake that excites the least stable spatial mode of the mean wake flow.^{24,25} We describe the numerical method and scope of the work in section II, before presenting our results in section III. We will focus on presenting and analyzing results at parameters where the pitching motion triggers, strengthens, and interferes with vortex shedding.

II. Numerical method and scope of investigation

We use an immersed boundary projection method^{26,27} to perform direct numerical simulations of the incompressible Navier–Stokes equations. The domain consists of four nested grids about a flat plate airfoil. A diagram of the computational domain is shown in Figure 1. Each of the four grids contains 600 by 300 grid points, with a total computational domain extending 96 and 48 chord lengths in the streamwise and transverse directions, respectively. The Reynolds number (based on chord length and freestream velocity) is fixed at 100 throughout. The relative computational cheapness of such two-dimensional, low Reynolds number configurations makes thorough investigations of high-dimensional parameter spaces feasible. Resolution studies were performed to ensure that the resolution and extent of the domain were sufficient. Crank-Nicholson and third-order Runge-Kutta time steppers were used to evolve the linear and nonlinear terms respectively, with step size ranging between $\Delta t = 0.0005c/U$ and $\Delta t = 0.01c/U$, with the smaller range of Δt required to resolve pitching motions with larger frequencies and/or amplitudes. In all cases, we run the simulations for sufficiently long such that any limit cycle or long-time behavior is reached before the data that is used for analysis is collected. We consider airfoil kinematics of the form

$$\alpha(t) = \alpha_M + \alpha_A \sin(2\pi f^* t), \quad (1)$$

where $f^* = fc/U$ is a dimensionless frequency. We perform simulations with the mean angle of attack varying in 5° increments between 15° and 45° , with pitching amplitudes of 1° , 2° , 5° and 10° . We consider frequencies in the range $f^* \in [0.01, 5]$, with approximately 20 frequencies used for each α_M and α_A . For some cases, additional frequencies are added to improve local resolution in parameter space. Performing these simulations with for pitching about the leading edge and midchord, this results in a total of approximately 1120 individual simulations.

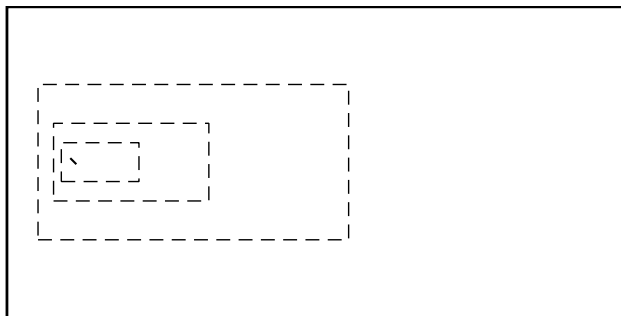


Figure 1. Computational domain used for this study, with the size and location of the airfoil shown. Dashed lines represent the borders of each nested grid.

III. Results

III.A. Static data

To give a sense for the behavior of the stationary airfoil, we show a typical lift curve in Figure 2. We observe the expected linear relationship between the angle of attack, α , and the lift coefficient, C_L for low angles of attack. Once the angle of attack becomes sufficiently large ($\alpha > 10^\circ$), flow separation on the upper surface of the airfoil leads to a shallow lift slope. At $\alpha \approx 20^\circ$, the flow is separated and steady. Beyond a critical angle of attack $\alpha_c \approx 27^\circ$, the steady solution becomes unstable, and periodic vortex shedding is observed.

This is an example of a supercritical Hopf bifurcation that is seen in the wake of bluff bodies as the Reynolds number is increased.²⁸ Note that in the case of an airfoil at an angle of attack, the projected area $c \sin(\alpha)$ is the effective length parameter for determining the location of the bifurcation. For $\alpha > \alpha_c$, the system exhibits higher lift (and drag) than would occur at the unstable equilibrium solution.

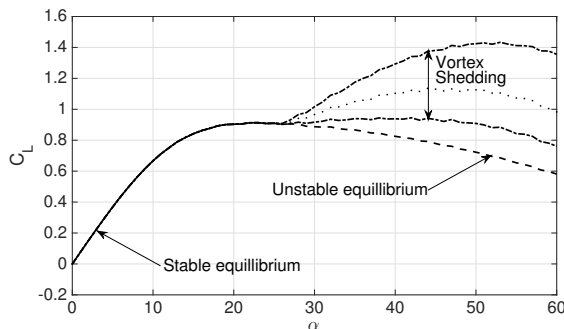


Figure 2. Lift curve for stationary airfoil, showing regions where the equilibrium is stable ($\alpha < 27^\circ$) and unstable ($\alpha > 27^\circ$), above which periodic vortex shedding occurs.

III.B. Force analysis

In this section, we study the lift and drag forces for pitching motion with various amplitudes, frequencies, and mean angles of attack.

Figure 3 shows the mean lift coefficient as a function of the dimensionless frequency, f^* , for pitching with a range of amplitudes, α_A , and mean angles of attack, α_M . We observe a distinct local peak in C_L for all values of α_M and α_A , aside from pitching with low amplitudes ($\alpha_A = 1^\circ$ or 2°) about $\alpha_M = 15^\circ$. The location of this lift peak moves slightly as α_M varies, from approximately $f^* = 0.3$ at $\alpha_M = 20^\circ$, to $f^* = 0.23$ at $\alpha_M = 45^\circ$. For $\alpha_M \geq 30^\circ$, we observe a second peak emerging at approximately twice the frequency of the dominant peak. This suggests that we excite dynamics that give enhanced lift when pitching at both a fundamental frequency and its first harmonic. We note also that the size of the lift increment seems to be largest for the intermediate base angles of 25° and 30° .

Figure 4 shows the mean drag coefficient for the same range of parameters as Figure 3. We find that there are increases in drag that show similar behavior to those for the lift. To compare the changes in lift and drag more explicitly, we plot the ratio between mean lift and drag coefficients in Figure 5. For larger pitching amplitudes, there is an increase in the lift-to-drag ratio at certain frequencies. The frequency of the lift-to-drag peak shows similar behavior to the peaks in both lift and drag (note that, unlike the lift and drag forces, lift over drag decreases with increasing α_M). This finding is potentially important for the effectiveness of such motions in flight.

Turning our attention back to the lift coefficient, we plot in Figure 6 the increase in lift coefficient from the fixed-wing value at α_M , normalized by the amplitude of pitching. For angles of attack below the critical angle (α_c) at which vortex shedding occurs, the lift increment is slightly larger for larger α_A , even after normalizing, despite the fact that the mean lift is lower than the fixed-wing value across other frequencies. This could be due to the fact that, for larger α_A , the maximum angle of attack attained in a pitching cycle is closer to or exceeds α_c , and thus better able to excite vortex shedding. Conversely, for $\alpha_M \geq 25^\circ$, the normalized lift increment is slightly larger for smaller pitching amplitudes, though in some cases this is in line with the larger average lift increments present for lower pitching amplitudes across all frequencies.

To analyze the effect of pitch axis location, we show in Figure 7 the normalized lift increment (i.e., the same quantity plotted in Figure 6) for pitching about the leading edge, rather than the midchord. We find very similar results to pitching about the midchord, with maximum increased lift at dimensionless frequencies between 0.25 and 0.3. The lift increment is larger for pitching about the leading edge, which could be due to the increased range of motion of the trailing edge for the same angular pitch amplitude. Note also that

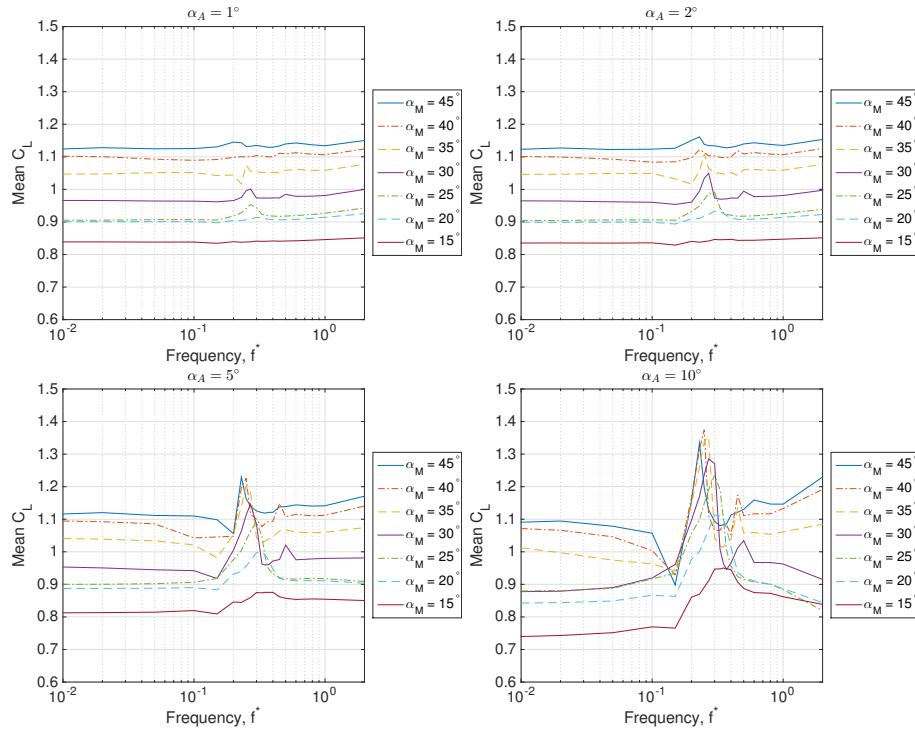


Figure 3. Mean lift coefficient for a range of pitching amplitudes α_A , frequencies, f^* , and mean angles of attack, α_M . Pitching is about the midchord.

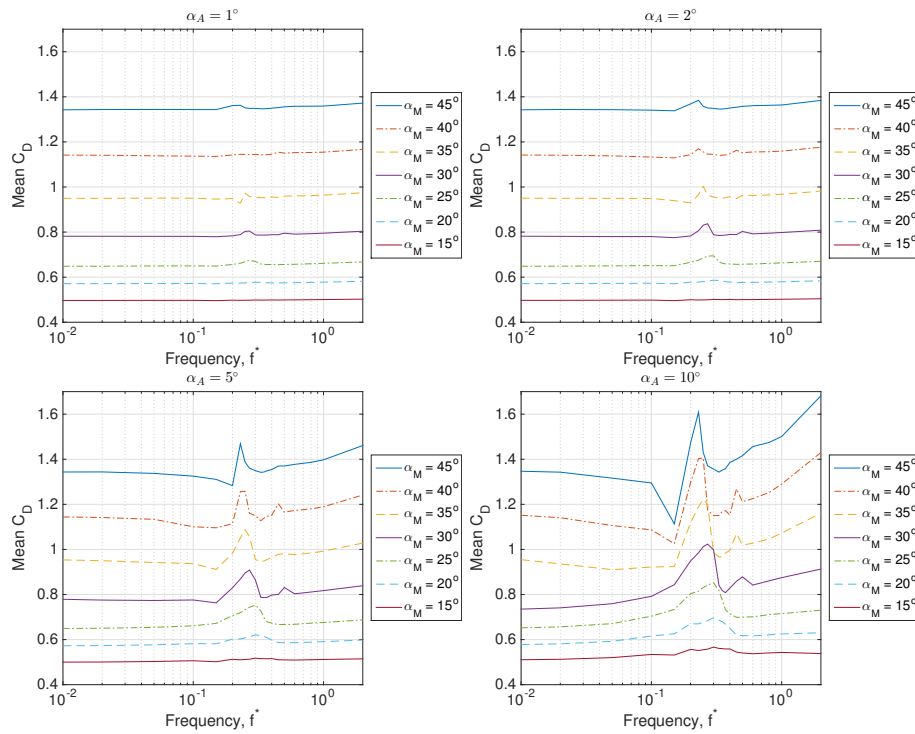


Figure 4. Mean drag coefficient for a range of pitching amplitudes α_A , frequencies, f^* , and mean angles of attack, α_M . Pitching is about the midchord.

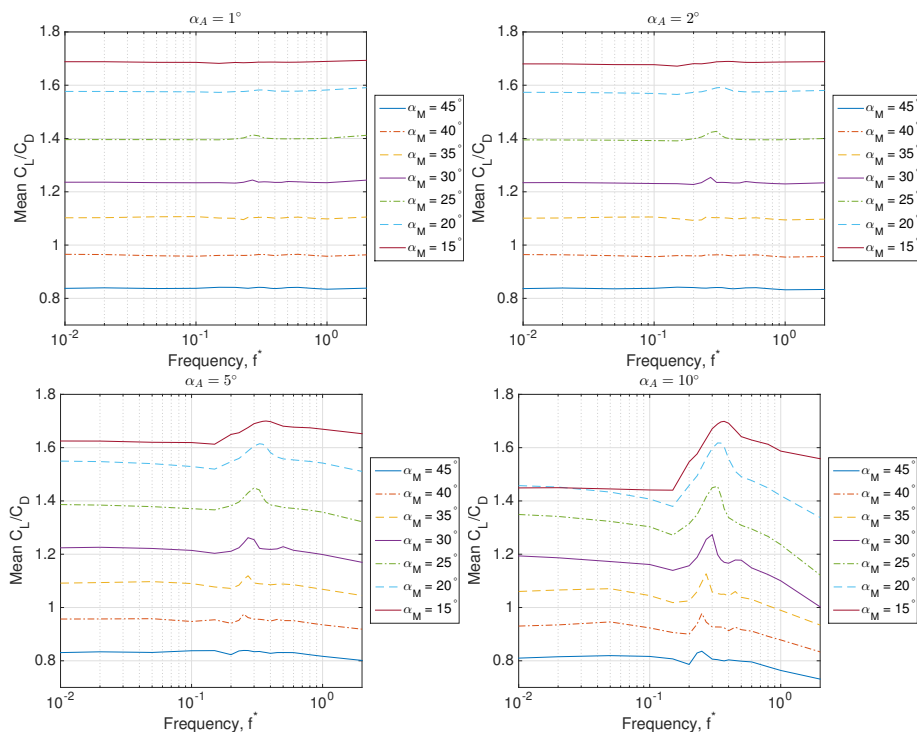


Figure 5. Mean of lift-to-drag ratio for a range of pitching amplitudes α_A , frequencies, f^* , and mean angles of attack, α_M . Pitching is about the midchord.

leading edge pitching will result in larger added mass forces, which for nonzero α_M will increase lift and decrease drag, particularly for high pitching frequencies. The remainder of this section will consider pitching about the midchord. The effect of pitch axis location will be investigated more thoroughly in the next section.

Figure 8 indicates how the mean lift compares to the maximum and minimum lift for $\alpha_A = 5^\circ$. Note that in some of the cases the lift is not periodic with the period of forcing, so these maximum and minimum values are the global extrema over many cycles. We observe (particularly clearly for lower mean angles of attack) that as the frequency increases from low values, the amplitude of the lift response increases, while the mean remains approximately constant. Above $f^* \approx 0.2$, the amplitude of the variation in lift decreases, but with the lift minimum rising more abruptly than the lift maximum falls. This asymmetry produces the higher average lift that is observed in the range $0.1 < f^* < 0.5$. For higher frequencies, larger added mass forces mean that the amplitude of the lift oscillations continue to increase, though the mean lift stays approximately constant.

To analyze the time-varying behavior in more detail, we take the discrete Fourier transform of the lift coefficient signal in time for each trial. The results for this are shown in Figure 9, for pitching amplitude $\alpha_A = 1^\circ$. For $\alpha_M \leq 25$, we observe one dominant frequency peak, corresponding to the pitching frequency f^* . Even though the undisturbed wake is stable at $\alpha = 25^\circ$, we still observe some frequency content near the almost-unstable vortex shedding mode across all pitching frequencies. For larger angles of attack, there is a second major peak in the spectra, corresponding to the vortex shedding frequency at the given α_M . In the region where these two frequencies are similar, there appear to be complex interactions between the dynamics associated with each frequency. As α_M grows larger, a distinct peak emerges at the first harmonic of the fundamental vortex shedding frequency, further complicating the frequency response of the system, which can now include, at very least, sums and differences of multiples of these frequencies.

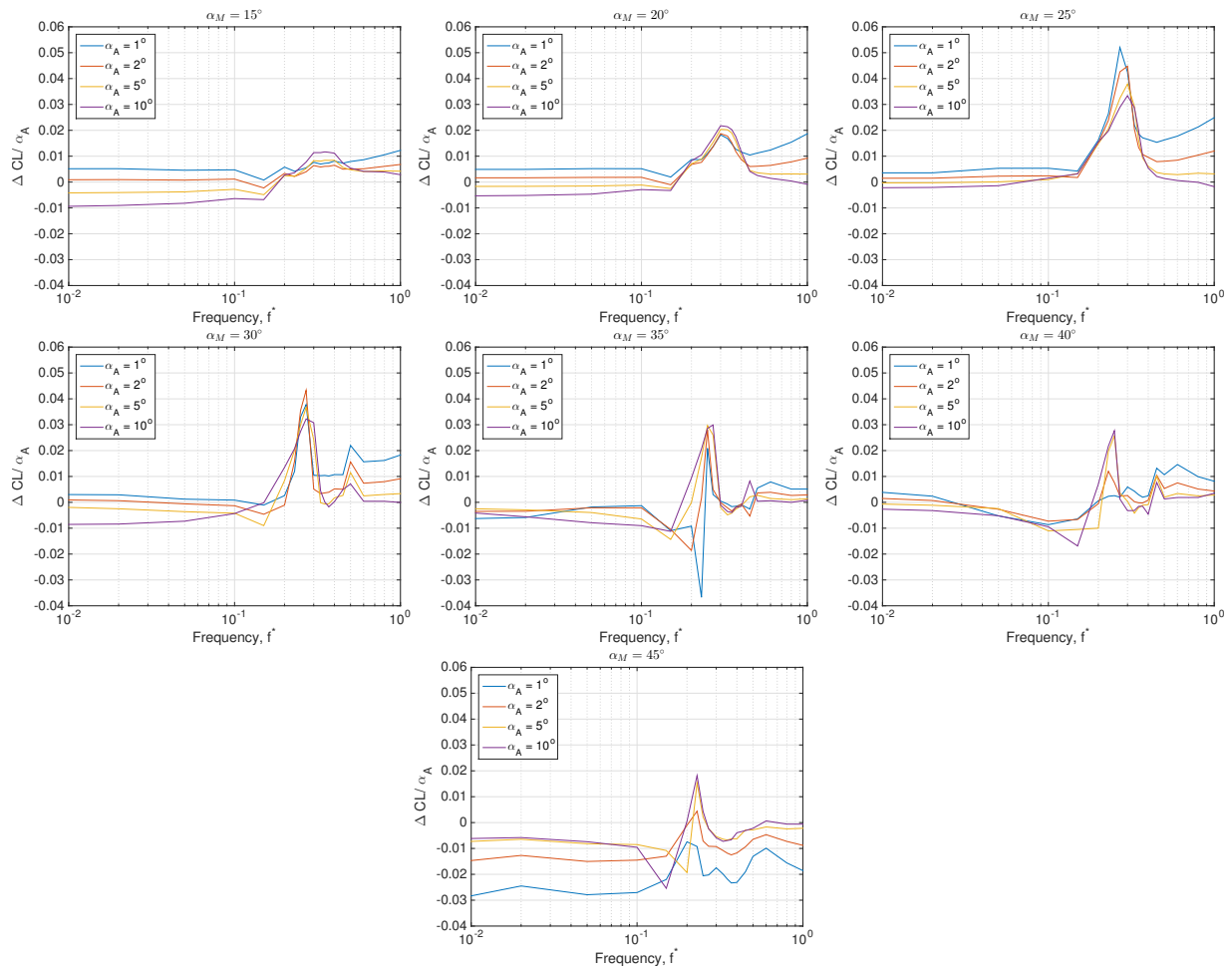


Figure 6. Mean lift coefficient increment over the fixed airfoil value, normalized by the amplitude of pitching α_A , across a range of pitching amplitudes α_A , frequencies, f^* , and mean angles of attack, α_M . Pitching is about the midchord.

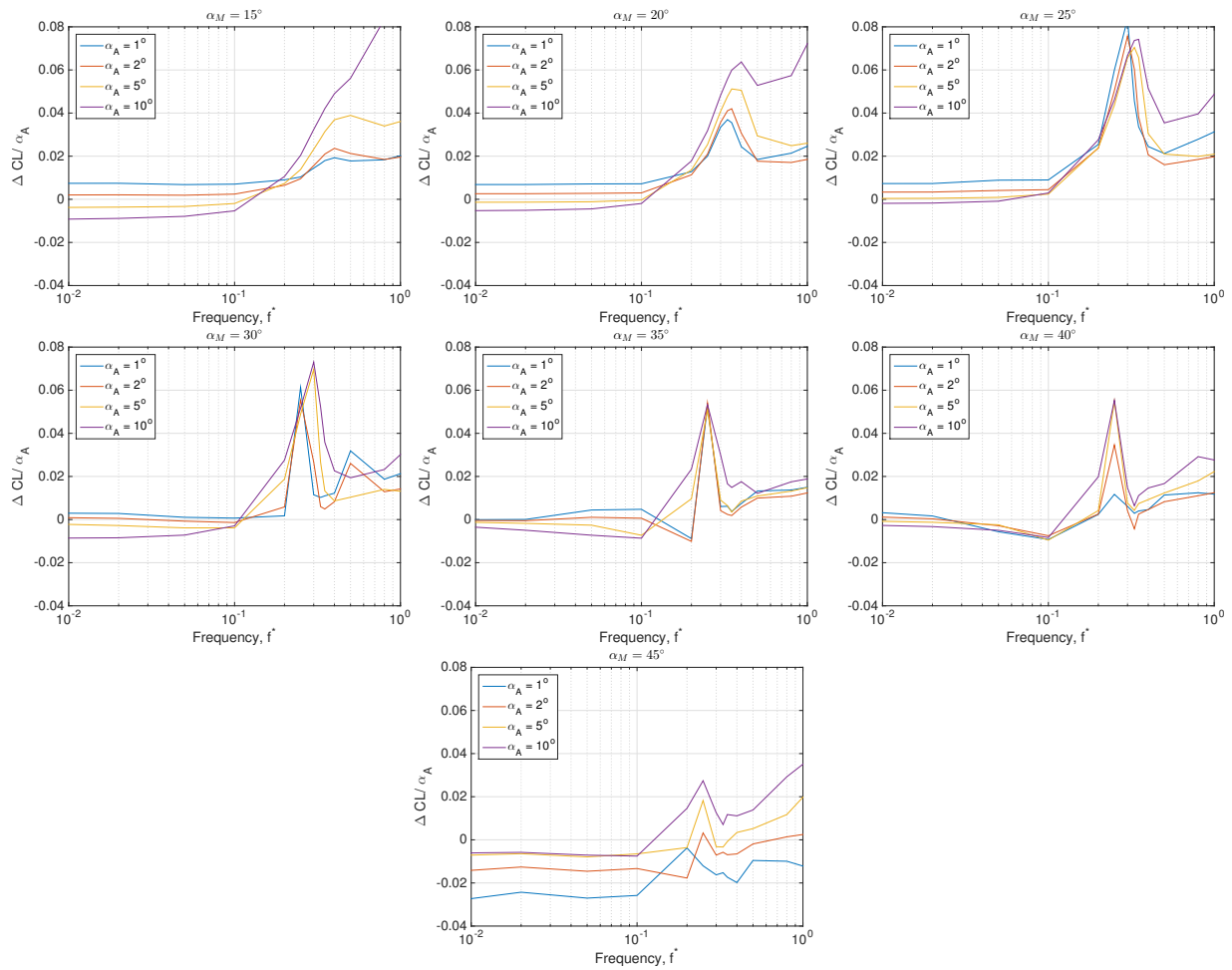


Figure 7. Mean lift coefficient increment over the fixed airfoil value, normalized by the amplitude of pitching α_A , across a range of pitching amplitudes α_A , frequencies, f^* , and mean angles of attack, α_M . Pitching is about the leading edge.

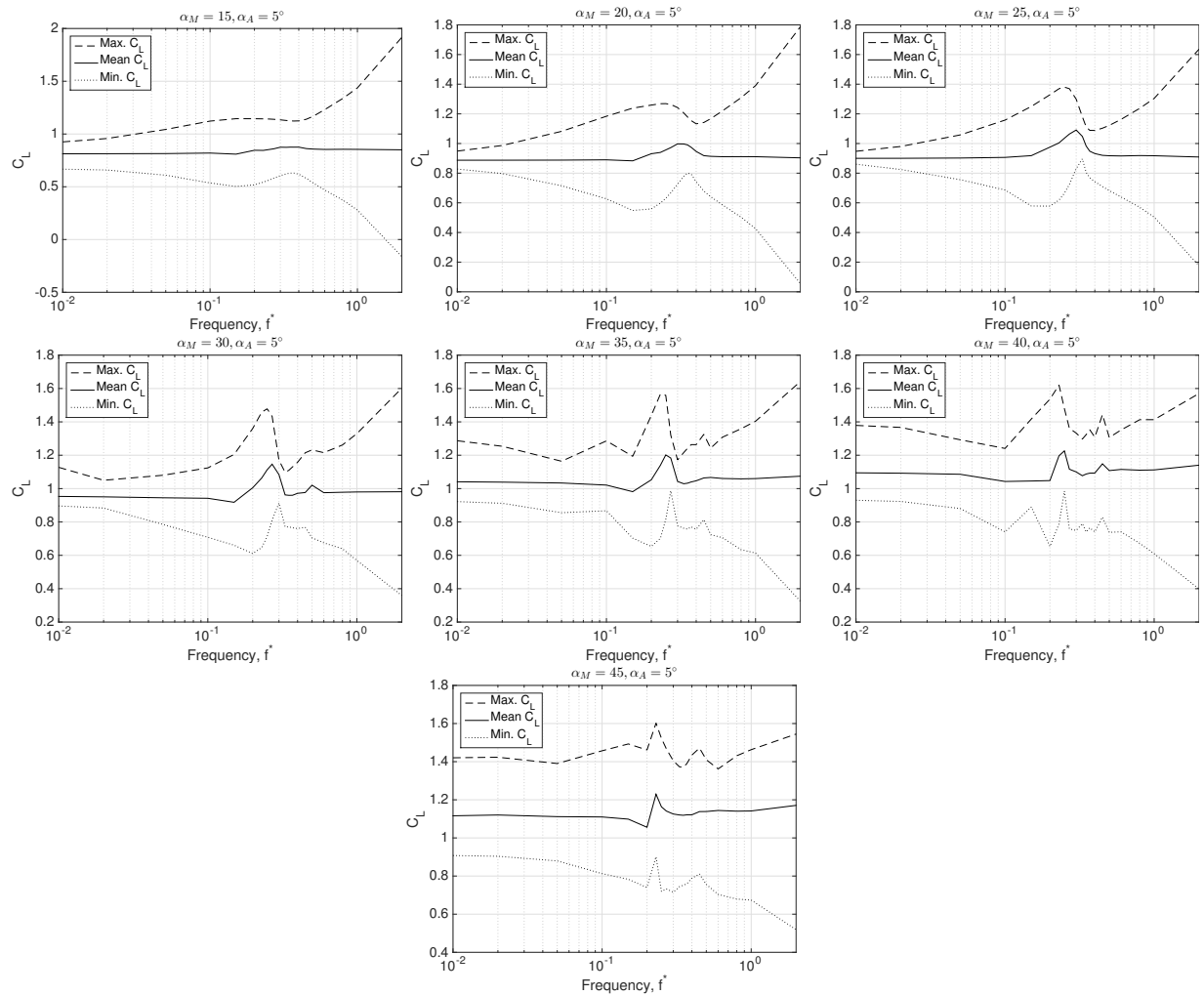


Figure 8. A comparison between the maximum, minimum, and mean lift coefficient attained for pitching with amplitude $\alpha_A = 5^\circ$, for a range of mean angles of attack, α_M , and frequencies, f^* . Pitching is about the midchord.

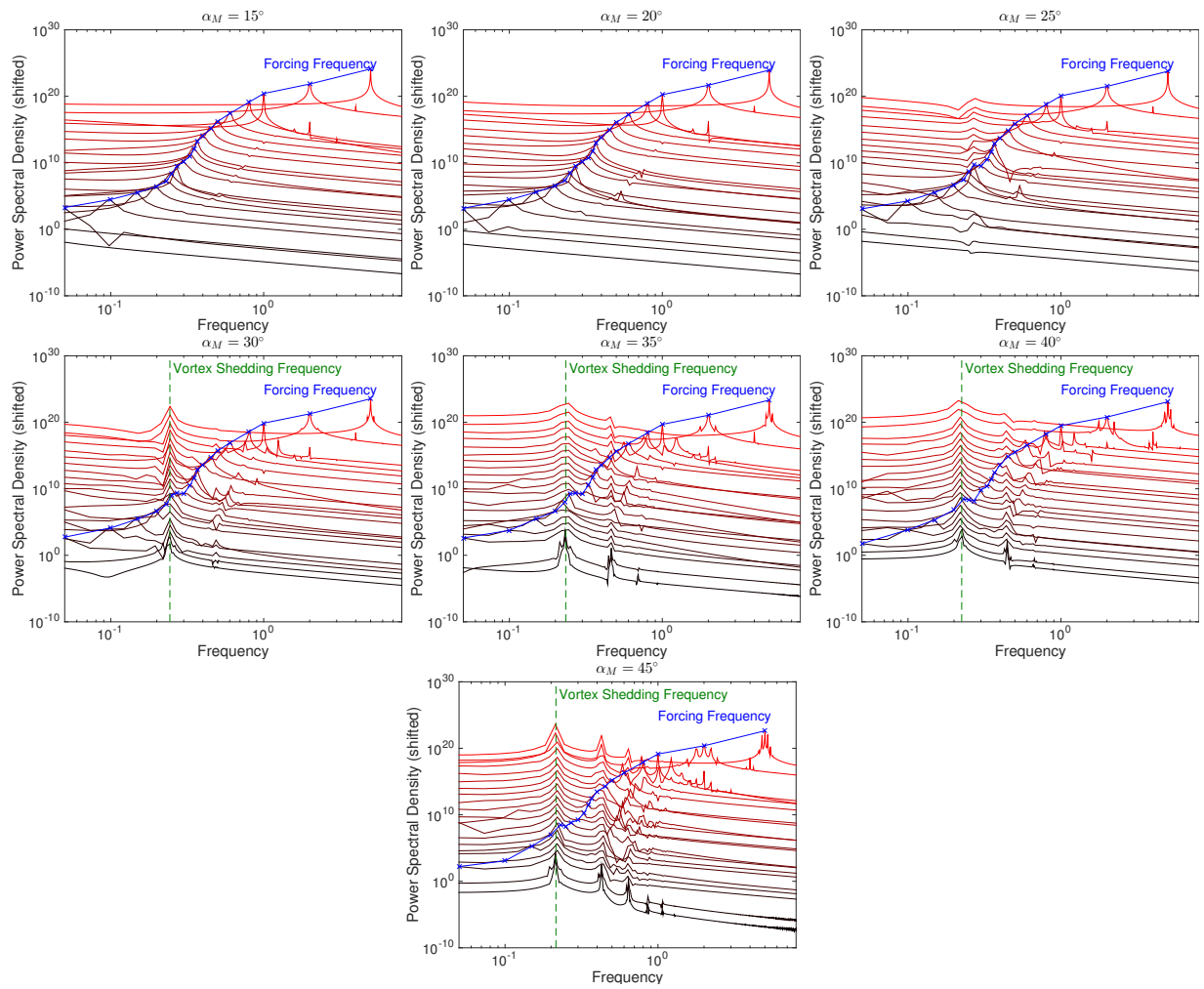


Figure 9. Power spectral densities of the lift force for pitching motion about the midchord with amplitude $\alpha_A = 1^\circ$. For clarity, the spectra for each forcing frequency is shifted by one order of magnitude, so the absolute scale of the vertical axis is not significant.

III.C. Wake analysis with dynamic mode decomposition

Here we analyze the flow field in the wake of the body, in an attempt to study the underlying physics behind the phenomena observed in section III.B. We will make use of the dynamic mode decomposition (DMD)^{29, 30} which is a technique that can extract dynamical content from data, in the form of spatial modes and their associated growth/decay rates and frequencies of oscillation. We refer the reader to recent references for details of the DMD algorithm^{30, 31, 32, 33} and its variants.^{34, 35, 36, 37, 38, 39}

We begin by considering a base angle $\alpha_M = 20^\circ$, which is prior to the Hopf bifurcation at which unforced vortex shedding occurs, and thus has a stable equilibrium wake. Figure 10 shows vorticity field snapshots for a variety of forcing frequencies with amplitude $\alpha_A = 1^\circ$. We observe that at around $f^* \approx 0.3$, the vorticity field is qualitatively different, with periodic vortex shedding being excited by the pitching motion. This immediately suggests that the increased lift observed at these pitching frequencies arises due to enhanced vortex formation. We note that the vorticity fields for pitching about the leading edge (left) and midchord (right) show similar results, with leading-edge pitching generally leading to stronger, more distinct vortices forming closer to the airfoil.

The vorticity fields shown in Figure 11 have the same parameters as those for Figure 10, but with a larger pitching amplitude of $\alpha_A = 5^\circ$. We again see the same phenomena where the forcing excites vortex shedding, but here distinct vortices form and persist downstream over a wider range of frequencies. This is consistent with the results from section III.B, where for the $\alpha_M = 20^\circ$ case in Figures 3 we observe an enhanced lift over a wider range of frequencies for higher forcing amplitudes.

To investigate further the dynamics of the wakes, we perform DMD on the vorticity field. We use 191 snapshots for each case, with a time gap between snapshots of $\Delta t = 0.1c/U$. We take data from a region downstream of the body as our domain for DMD, to avoid complications associated with having the moving body in the domain. For clarity of results, we truncate the rank of our data to 20 proper orthogonal decomposition (POD)⁴⁰ modes. This is found to capture at least 99% of the energy of the flow.

While it is most often applied to data from systems without external forcing, DMD can be used to examine forced systems,^{41, 42, 43} though one must take care in the interpretation of its outputs. In this context, we show that it can be an effective tool to determine both the frequency content of the wake, and also if the wake “locks on” to a vortex shedding mode. As an aside, we note that more rigorous connections between DMD and Fourier analysis can be made.³⁴

Figure 12 shows the DMD eigenvalues, as well as the four largest amplitude modes, for a variety of forcing frequencies, for pitching about the leading edge (left) midchord (right) with amplitude $\alpha_A = 1^\circ$. In this section, we restrict our attention to frequencies near the vortex shedding frequency and frequency of maximum lift. Results at lower and higher frequencies are similar to the minimum and maximum frequencies considered here. Note that the real and imaginary components of the eigenvalues (in continuous time) indicate the growth rate and frequency of the associated DMD modes.

For this mean angle of attack ($\alpha_M = 20^\circ$), the maximum increase in lift occurs at $f^* = 0.3$. At this frequency, the DMD eigenvalues are at the frequency of pitching and its harmonics. Since vortex shedding is clearly observed in Figure 10, this suggests that it is locking onto the forcing frequency. For the surrounding frequencies ($f^* = 0.25$ and 0.35), we observe that the eigenvalues are scattered across a range of frequencies. This suggests that vortex shedding is not fully locking on to the forcing frequency, and that there is a broad range of frequency content present. We also find that the second, third and fourth DMD modes all have similar spatial wavelength, again indicating that certain features persist across a range of frequencies. Note that, unlike POD modes, DMD modes are not required to be orthogonal, and thus there can exist multiple DMD modes that are similar to each other, having slightly different frequencies of oscillation.

If we move further away from $f^* = 0.3$, we find that the DMD modes again lie on harmonics of the forcing frequency. In these cases (i.e., for $f^* = 0.2$ and 0.4 plotted here, and for other cases not shown), it appears that the least stable mode in the wake is not being excited, as we are not close enough in frequency to do so. This also explains why there is no significant lift increase at these frequencies. The similarity between pitching at the leading edge and midchord suggests that these observations are not particularly sensitive to pitch-axis location.

Figure 13 shows plots of the same quantities and parameters as Figure 12, but for pitching with amplitude $\alpha_A = 5^\circ$. Broadly speaking, the results are similar, with DMD eigenvalues lying on the imaginary axis at multiples of the forcing frequency for $f^* = 0.2, 0.3$ and 0.4 , and located in a significantly more scattered

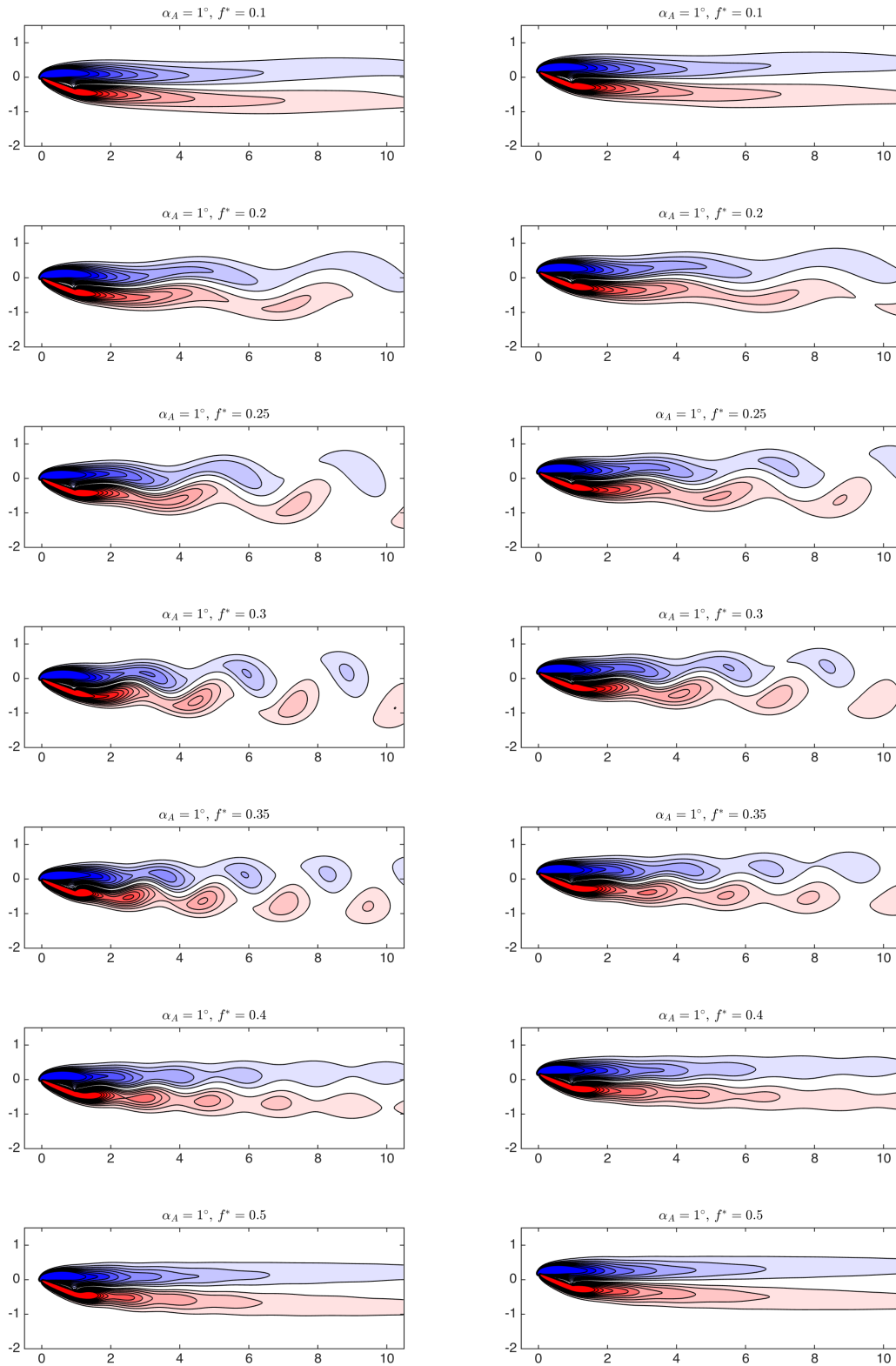


Figure 10. Instantaneous vorticity fields for pitching about the leading edge (left) and midchord (right) at a variety of frequencies, with $\alpha_M = 20^\circ$ and $\alpha_A = 1^\circ$.

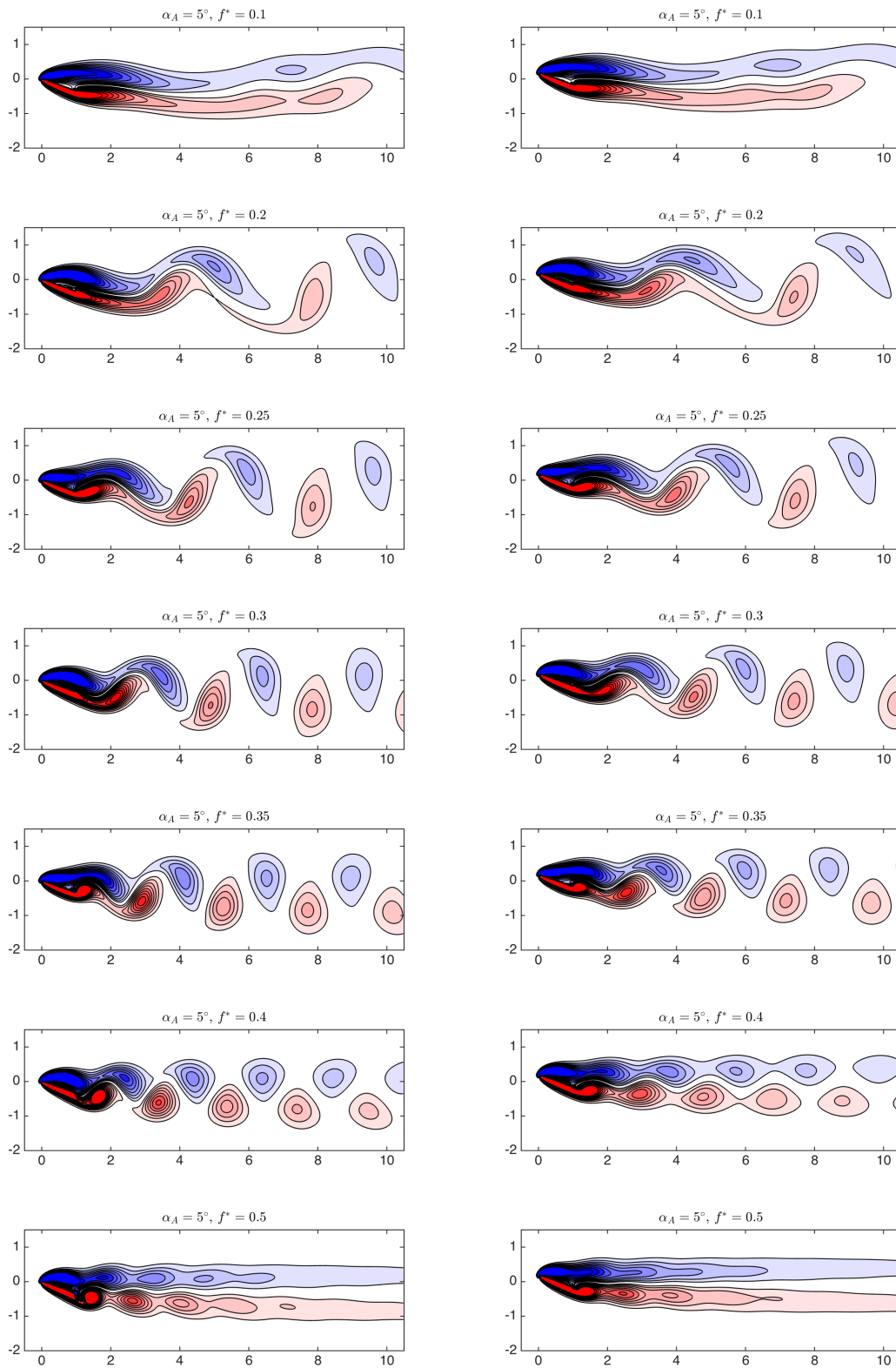


Figure 11. Instantaneous vorticity fields for pitching about the leading edge (left) and midchord (right) at a variety of frequencies, with $\alpha_M = 20^\circ$ and $\alpha_A = 1^\circ$.

arrangement with numerous modes of similar frequency content and spatial structure for $f^* = 0.25$ and 0.35 . We find that the oscillating modes have higher amplitude in this case, with the “lock-on” mode having higher amplitude than the mean mode for leading edge pitching at $f^* = 0.3$. We further note that, unlike the case for $\alpha_A = 1^\circ$, the mean flow (i.e., the DMD mode with a corresponding eigenvalue close to 0) looks substantially different between low frequency oscillation, where the wake seems to spread out substantially a short distance downstream of the airfoil, and high frequency oscillation, where the wake appears to be narrower with regions of high vorticity persisting far downstream. Referring back to Figure 11, the enhanced spreading of the mean flow is seemingly due to the larger vortices drifting above (for negative vorticity) and below (positive vorticity) the airfoil as they are shed. This phenomenon could also explain why the lift-to-drag ratio is often maximized at pitching frequencies slightly larger than those at which maximum lift occurs. The enhanced spreading at lower frequencies increases drag, so lift-to-drag benefits exist only at higher frequencies, where the wake remains thinner.

Thus far, we have only analyzed the wake for a case where the base flow is stable. We now turn our attention to the case, $\alpha_M = 30^\circ$, where the flow exhibits a vortex shedding limit cycle. Figure 14 shows vorticity field snapshots, as well as DMD eigenvalues and modes (only showing the four highest amplitude modes) for pitching about a mean angle $\alpha_M = 30^\circ$ with amplitude $\alpha_A = 1^\circ$, for a variety of pitching frequencies. The wakes for $f^* = 0.2, 0.3, 0.35$ and 0.4 all look very similar, with high amplitude DMD eigenvalues at the natural vortex shedding frequency, and lower amplitude eigenvalues at the pitching frequency. This is consistent with Figure 9, where the subplot for $\alpha_M = 30^\circ$ shows a larger peak at the vortex shedding frequency, and a lower peak at the forcing frequency. For $f^* = 0.25$, the forcing and vortex shedding frequencies are almost identical, which appears to give stronger vortex formation, and in turn the increase in lift seen in Figure 3.

IV. Discussion and conclusions

For angles of attack below the critical angle where unforced vortex shedding first occurs (α_c), it was found that pitching at a certain frequency can excite vortex shedding in the wake, leading to higher mean lift. The magnitude and width in frequency range of the lift increment increases significantly as the forcing amplitude increases. This is perhaps a similar phenomenon to the widening of the “resonance horn”⁴⁴ observed by Choi et al.¹⁷ for the case of a surging and plunging airfoil (though in that case, the system was above the critical bifurcation parameter). Note, however, that comparing Figures 3 and 13 indicates that there can be a significant increase in lift even without frequency lock-on.

For α_M above the critical angle for vortex shedding, there is a similar peak in the mean lift coefficient when the pitching frequency is close to the natural vortex shedding frequency or its first harmonic. When the natural and forcing frequencies are different, the interactions between the two frequencies can lead to complex frequency spectra in the forces and wakes. Note in particular that pitching some amount below the vortex shedding frequency can lead to a notable decrease in mean lift for $\alpha_A \geq 5^\circ$ at $\alpha_M \geq 35^\circ$.

While periodic pitching at the preferred frequency where vortex shedding is excited or enhanced also leads to an increase in drag, the differences in effect that pitching has on the two force components leads to an increase in the lift-to-drag ratio for frequencies slightly above the frequency for which the lift is maximized. It is interesting to note that while the frequency at which the maximum lift increment occurs decreases slightly as α_M increases (in agreement with the slight decrease in natural vortex shedding frequency), the frequency giving maximum lift-to-drag ratio increases with α_M . Indeed, for high α_M it seems that the maximum lift-to-drag ratio typically occurs between the peaks in lift and drag located at the vortex shedding frequency and its first harmonic, where there is a local lift minimum, and thus also a slightly more substantial drag minimum.

Beyond α_c , the interactions between the pitching and vortex shedding frequencies can lead to complex frequency spectra in both the forces (as seen in Figure 9) and wakes (Figures 12-14). There are numerous methods by which one can analyze frequency content, and here we show how DMD can clearly distinguish between cases where all frequencies present are harmonics of the pitching frequency, and where there is a broad range of frequency content.

There has been much effort in the past to understand, model, and predict unsteady aerodynamic forces, moments, pressures, and indeed many other quantities of interest for moving airfoils. Particularly in the

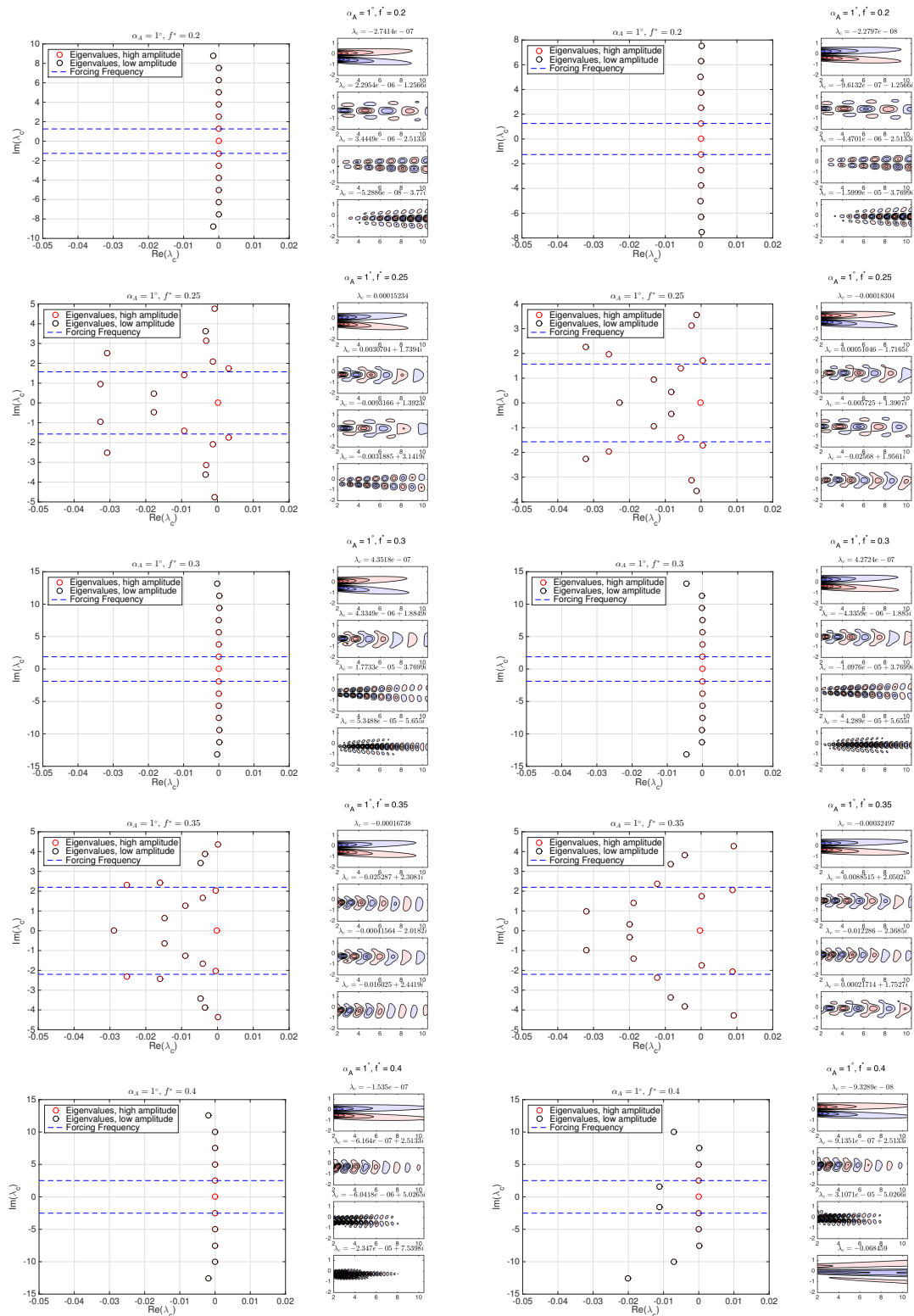


Figure 12. DMD eigenvalues, and the real components of the 4 largest amplitude modes (ordered by amplitude), for pitching about the leading edge (left), and midchord (right) at a variety of frequencies, with amplitude $\alpha_A = 1^\circ$, and mean angle of attack $\alpha_M = 20^\circ$. Eigenvalues that are colored red correspond to modes with larger amplitudes.

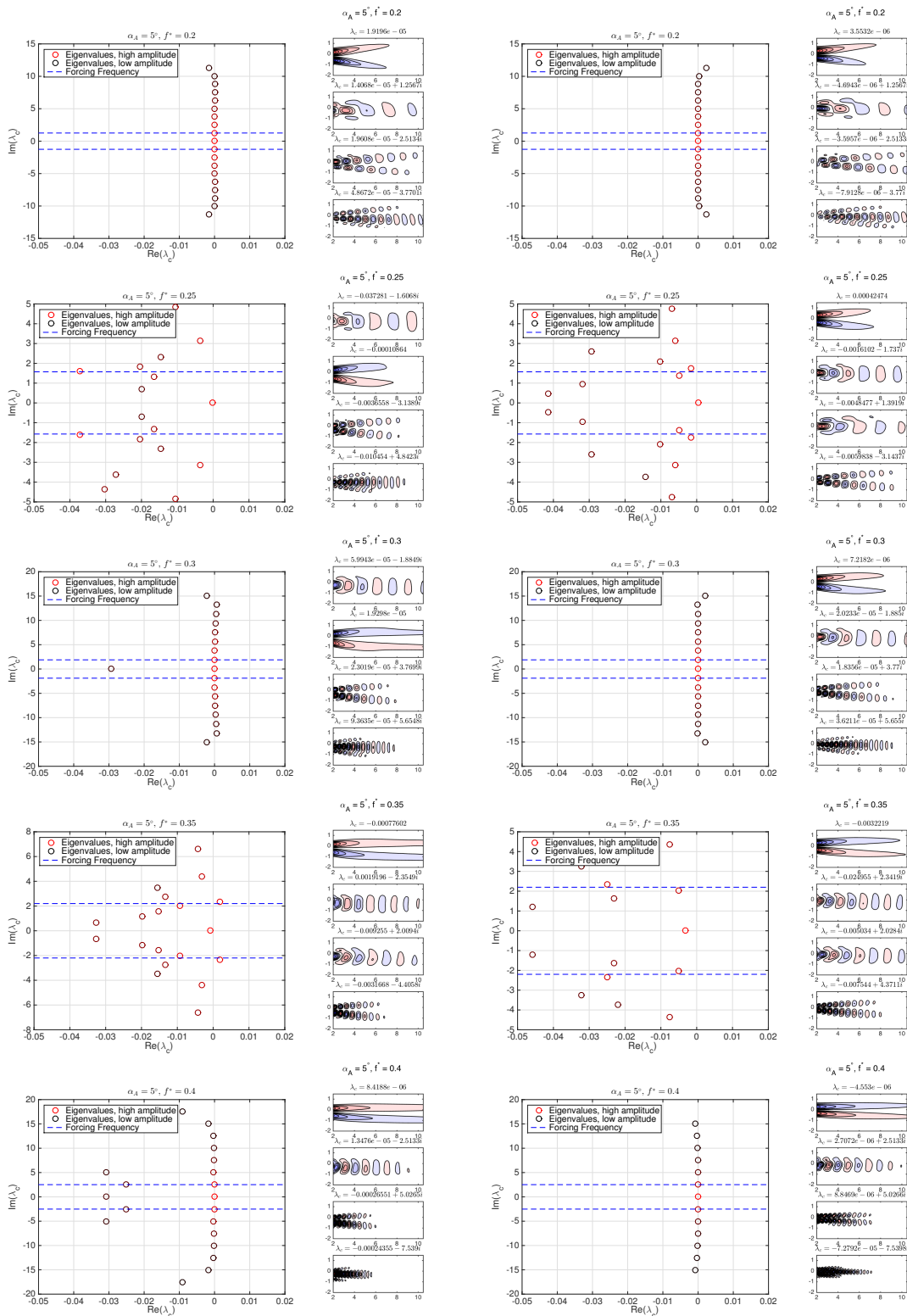


Figure 13. DMD eigenvalues, and the real components of the 4 largest amplitude modes (ordered by amplitude) for pitching about the leading edge (left), and midchord (right) at a variety of frequencies, with amplitude $\alpha_A = 5^\circ$, and mean angle of attack $\alpha_M = 20^\circ$. Eigenvalues that are colored red correspond to modes with larger amplitudes.

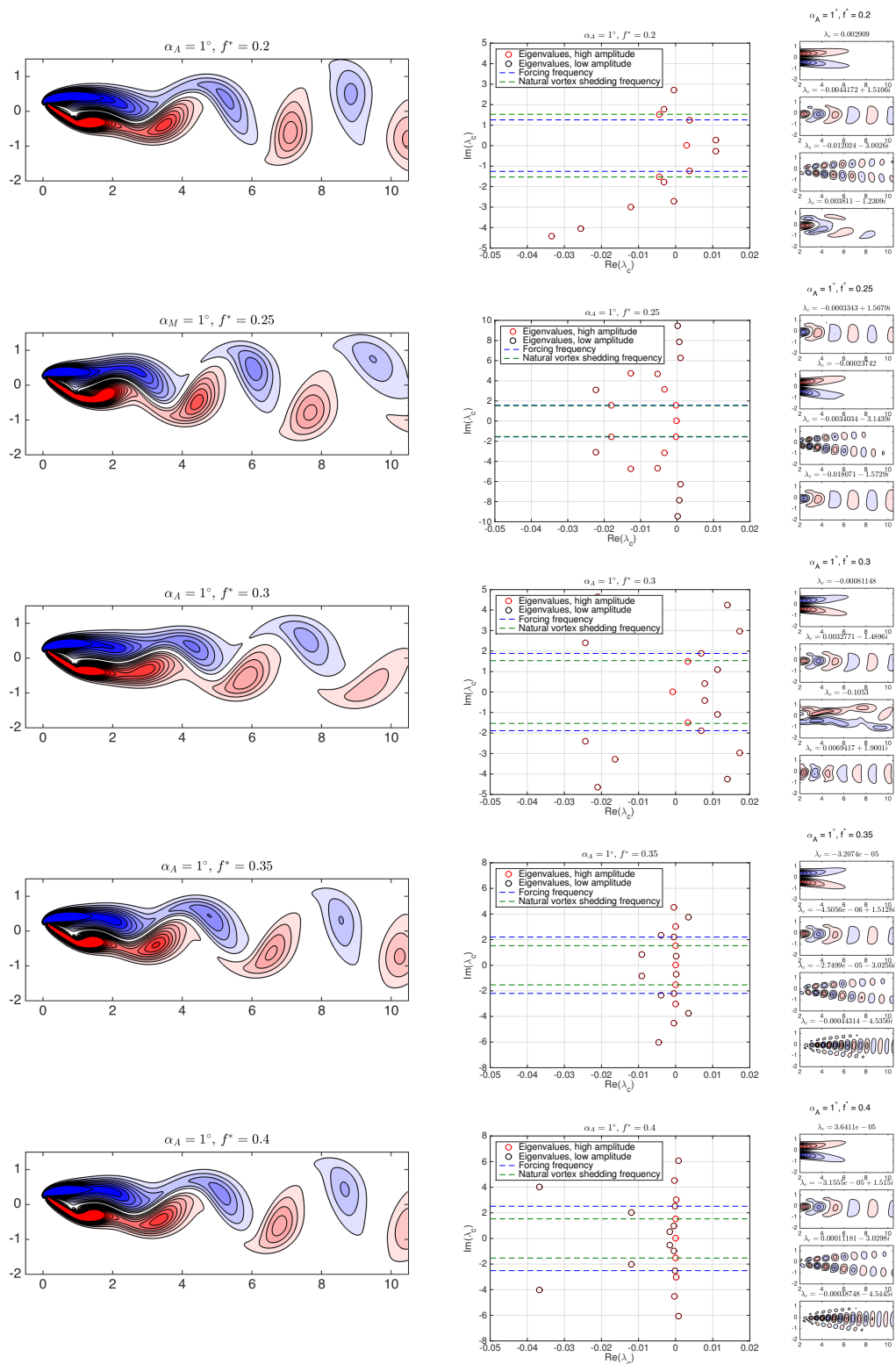


Figure 14. Wake snapshots, DMD eigenvalues, and the real components of the 4 largest amplitude modes (ordered by amplitude), for midchord pitching at a variety of frequencies, with amplitude $\alpha_A = 1^\circ$, and mean angle of attack $\alpha_M = 30^\circ$. Eigenvalues that are colored red correspond to modes with larger amplitudes.

case of separated flow, these dynamics are often highly nonlinear. One might seek to get around this by linearizing about a certain fixed point (say an angle of attack), in the hope that a linear model would at least be locally accurate. The findings presented here suggest that such an approach might be problematic, since a linear model (e.g., a transfer function) can only predict the magnitude and phase of a response to sinusoidal forcing, but not any change in the mean value. Thus, such effects must be accounted for separately, or a more complex modeling framework used.

Further work in this investigation will compare the findings to the results of stability analyses of the stable and unstable equilibrium wakes, and the mean of the vortex shedding wake, and will use wind tunnel experiments to investigate whether the phenomena observed persist for higher Reynolds numbers.

Acknowledgments

The authors acknowledge support from the Air Force Office of Scientific Research grant FA9550-14-1-0289.

References

- ¹Videler, J. J., Samhuis, E. J., and Povel, G. D. E., "Leading-edge vortex lifts swifts." *Science*, Vol. 306, 2004, pp. 1960–1962.
- ²Birch, J. and Dickinson, M., "Spanwise flow and the attachment of the leading-edge vortex on insect wings." *Nature*, Vol. 412, 2001, pp. 729–733.
- ³Sane, S. P., "The aerodynamics of insect flight." *The Journal of Experimental Biology*, Vol. 206, No. 23, 2003, pp. 4191–4208.
- ⁴Wang, Z. J., "Dissecting Insect Flight," *Annual Review of Fluid Mechanics*, Vol. 37, 2005, pp. 183–210.
- ⁵McCroskey, W., "Unsteady airfoils," *Annual review of fluid mechanics*, Vol. 14, No. 1, 1982, pp. 285–311.
- ⁶Brunton, S. L., Rowley, C. W., and Williams, D. R., "Reduced-order unsteady aerodynamic models at low Reynolds numbers," *Journal of Fluid Mechanics*, Vol. 724, 2013, pp. 203–233.
- ⁷Brunton, S. L., Dawson, S. T., and Rowley, C. W., "State-space model identification and feedback control of unsteady aerodynamic forces," *Journal of Fluids and Structures*, Vol. 50, 2014, pp. 253–270.
- ⁸Baik, Y. S., Bernal, L. P., Granlund, K., and Ol, M. V., "Unsteady force generation and vortex dynamics of pitching and plunging aerofoils," *Journal of Fluid Mechanics*, Vol. 709, 2012, pp. 37–68.
- ⁹Granlund, K. O., Ol, M. V., and Bernal, L. P., "Unsteady pitching flat plates," *Journal of Fluid Mechanics*, Vol. 733, 2013, pp. R5.
- ¹⁰Hemati, M. S., Eldredge, J. D., and Speyer, J. L., "Improving vortex models via optimal control theory," *Journal of Fluids and Structures*, Vol. 49, 2014, pp. 91–111.
- ¹¹Dawson, S. T. M., Schiavone, N. K., Rowley, C. W., and Williams, D. R., "A Data-Driven Modeling Framework for Predicting Forces and Pressures on a Rapidly Pitching Airfoil," *45th AIAA Fluid Dynamics Conference*, 2015, p. 2767.
- ¹²Zakaria, M. Y., Taha, H. E., Hajj, M. R., and Hussein, A. A., "Experimental-Based Unified Unsteady Nonlinear Aerodynamic Modeling For Two-Dimensional Airfoils," *33rd AIAA Applied Aerodynamics Conference*, 2015, p. 3167.
- ¹³Sarpkaya, T., "Vortex-induced oscillations: a selective review," *Journal of Applied Mechanics*, Vol. 46, No. 2, 1979, pp. 241–258.
- ¹⁴Young, J. and Lai, J. C., "Vortex lock-in phenomenon in the wake of a plunging airfoil," *AIAA journal*, Vol. 45, No. 2, 2007, pp. 485–490.
- ¹⁵Cleaver, D. J., Wang, Z., Gursul, I., and Visbal, M., "Lift enhancement by means of small-amplitude airfoil oscillations at low Reynolds numbers," *AIAA journal*, Vol. 49, No. 9, 2011, pp. 2018–2033.
- ¹⁶Cleaver, D., Wang, Z., and Gursul, I., "Investigation of high-lift mechanisms for a flat-plate airfoil undergoing small-amplitude plunging oscillations," *AIAA journal*, Vol. 51, No. 4, 2013, pp. 968–980.
- ¹⁷Choi, J., Colonius, T., and Williams, D. R., "Surging and plunging oscillations of an airfoil at low Reynolds number," *Journal of Fluid Mechanics*, Vol. 763, 2015, pp. 237–253.
- ¹⁸Cleaver, D. J., Wang, Z., and Gursul, I., "Bifurcating flows of plunging aerofoils at high Strouhal numbers," *Journal of Fluid Mechanics*, Vol. 708, 2012, pp. 349–376.
- ¹⁹Milano, M. and Gharib, M., "Uncovering the physics of flapping flat plates with artificial evolution," *Journal of Fluid Mechanics*, Vol. 534, 2005, pp. 403–409.
- ²⁰Gharib, M., Rambod, E., and Shariff, K., "A universal time scale for vortex ring formation," *Journal of Fluid Mechanics*, Vol. 360, 1998, pp. 121–140.
- ²¹Taira, K. and Colonius, T., "Three-dimensional flows around low-aspect-ratio flat-plate wings at low Reynolds numbers," *Journal of Fluid Mechanics*, Vol. 623, 2009, pp. 187–207.
- ²²Tregidgo, L., Wang, Z., and Gursul, I., "Frequency lock-in phenomenon for self-sustained roll oscillations of rectangular wings undergoing a forced periodic pitching motion," *Physics of Fluids (1994-present)*, Vol. 24, No. 11, 2012, pp. 117101.
- ²³Dewey, P. A., Carriou, A., and Smits, A. J., "On the relationship between efficiency and wake structure of a batoid-inspired oscillating fin," *Journal of Fluid Mechanics*, Vol. 691, 2012, pp. 245–266.
- ²⁴Triantafyllou, M., Triantafyllou, G., and Gopalkrishnan, R., "Wake mechanics for thrust generation in oscillating foils," *Physics of Fluids A: Fluid Dynamics (1989-1993)*, Vol. 3, No. 12, 1991, pp. 2835–2837.

- ²⁵Triantafyllou, G., Triantafyllou, M., and Grosenbaugh, M., "Optimal thrust development in oscillating foils with application to fish propulsion," *Journal of Fluids and Structures*, Vol. 7, No. 2, 1993, pp. 205–224.
- ²⁶Taira, K. and Colonius, T., "The immersed boundary method: a projection approach." *Journal of Computational Physics*, Vol. 225, No. 2, 2007, pp. 2118–2137.
- ²⁷Colonius, T. and Taira, K., "A fast immersed boundary method using a nullspace approach and multi-domain far-field boundary conditions," *Computer Methods in Applied Mechanics and Engineering*, Vol. 197, 2008, pp. 2131–2146.
- ²⁸Sreenivasan, K., Strykowski, P., and Olinger, D., "Hopf bifurcation, Landau equation, and vortex shedding behind circular cylinders," *Forum on unsteady flow separation*, Vol. 1, 1987, pp. 1–13.
- ²⁹Schmid, P. J. and Sesterhenn, J., "Dynamic mode decomposition of numerical and experimental data," *61st Annual Meeting of the APS Division of Fluid Dynamics*, American Physical Society, 2008.
- ³⁰Schmid, P. J., "Dynamic mode decomposition of numerical and experimental data," *Journal of Fluid Mechanics*, Vol. 656, 2010, pp. 5–28.
- ³¹Rowley, C. W., Mezić, I., Bagheri, S., Schlatter, P., and Henningson, D. S., "Spectral analysis of nonlinear flows," *Journal of Fluid Mechanics*, Vol. 641, No. 1, 2009, pp. 115–127.
- ³²Tu, J. H., Rowley, C. W., Luchtenburg, D. M., Brunton, S. L., and Kutz, J. N., "On Dynamic Mode Decomposition: Theory and Applications," *Journal of Computational Dynamics*, Vol. 1, No. 2, 2014, pp. 391–421.
- ³³Williams, M. O., Kevrekidis, I. G., and Rowley, C. W., "A Data-Driven Approximation of the Koopman Operator: Extending Dynamic Mode Decomposition," *Journal of Nonlinear Science*, 2015, pp. 1–40.
- ³⁴Chen, K. K., Tu, J. H., and Rowley, C. W., "Variants of dynamic mode decomposition: boundary condition, Koopman, and Fourier Analyses," *Journal of Nonlinear Science*, Vol. 22, No. 6, 2011, pp. 887–915.
- ³⁵Wynn, A., Pearson, D. S., Ganapathisubramani, B., and Goulart, P. J., "Optimal mode decomposition for unsteady flows," *Journal of Fluid Mechanics*, Vol. 733, 2013, pp. 473–503.
- ³⁶Jovanović, M. R., Schmid, P. J., and Nichols, J. W., "Sparsity-promoting dynamic mode decomposition," *Physics of Fluids (1994-present)*, Vol. 26, No. 2, 2014, pp. –.
- ³⁷Hemati, M. S., Williams, M. O., and Rowley, C. W., "Dynamic mode decomposition for large and streaming datasets," *Physics of Fluids (1994-present)*, Vol. 26, No. 11, 2014, pp. 111701.
- ³⁸Hemati, M. S., Rowley, C. W., Deem, E. A., and Cattafesta, L. N., "De-Biasing the Dynamic Mode Decomposition for Applied Koopman Spectral Analysis," *arXiv preprint arXiv:1502.03854*, 2015.
- ³⁹Dawson, S. T. M., Hemati, M. S., Williams, M. O., and Rowley, C. W., "Characterizing and correcting for the effect of sensor noise in the dynamic mode decomposition," *arXiv preprint arXiv:1507.02264*, 2015.
- ⁴⁰Holmes, P., Lumley, J. L., Berkooz, G., and Rowley, C. W., *Turbulence, coherent structures, dynamical systems and symmetry*, Cambridge University Press, 2012.
- ⁴¹Tu, J. H., Rowley, C. W., Aram, E., and Mittal, R., "Koopman spectral analysis of separated flow over a finite-thickness flat plate with elliptical leading edge," *49th AIAA Aerospace Sciences Meeting and Exhibit*, AIAA, 2011, pp. AIAA–Paper.
- ⁴²Proctor, J. L., Brunton, S. L., and Kutz, J. N., "Dynamic mode decomposition with control," *arXiv preprint arXiv:1409.6358*, 2014.
- ⁴³Mohan, A. T., Visbal, M. R., and Gaitonde, D. V., *Model Reduction and Analysis of Deep Dynamic Stall on a Plunging Airfoil using Dynamic Mode Decomposition*, American Institute of Aeronautics and Astronautics, 2015/11/29 2015.
- ⁴⁴Boyland, P. L., "Bifurcations of circle maps: Arnol'd tongues, bistability and rotation intervals," *Communications in Mathematical Physics*, Vol. 106, No. 3, 1986, pp. 353–381.